

Fast and Accurate Semi-Automatic Segmentation Tool for Brain Tumor MRIs

Andrew X. Chen^a, Raúl Rabadán^{a,b,*}

^a*Department of Systems Biology, Columbia University Medical Center, 1130 St. Nicholas Avenue, New York, NY 10032, USA*

^b*Department of Biomedical Informatics, Columbia University Medical Center, 622 W. 168th Street, New York, NY 10032, USA*

Abstract

Segmentation, the process of delineating tumor apart from healthy tissue, is a vital part of both the clinical assessment and the quantitative analysis of brain cancers. Here, we provide an open-source algorithm (MITKats), built on the Medical Imaging Interaction Toolkit, to provide user-friendly and expedient tools for semi-automatic segmentation. To evaluate its performance against competing algorithms, we applied MITKats to 38 high-grade glioma cases from publicly available benchmarks. The similarity of the segmentations to expert-delineated ground truths approached the discrepancies among different manual raters, the theoretically maximal precision. The average time spent on each segmentation was 5 minutes, making MITKats between 4 and 11 times faster than competing semi-automatic algorithms, while retaining similar accuracy.

Keywords: Semi-automatic segmentation; Brain tumor; Glioblastoma; MRI; MITK

*Corresponding author

Email address: rr2579@cumc.columbia.edu (Raúl Rabadán)

1. Introduction

Glioblastoma (GBM) is the most common primary brain malignancy, and the one with the most dismal prognosis (DeAngelis, 2001). Imaging, particularly magnetic resonance imaging (MRI), is the standard for diagnosing and assessing the disease (Mabray et al., 2015). The delineation of tumor volumes within images, or segmentation, is important for guiding therapy (Dupont et al., 2016; Bauer et al., 2013a), determining prognosis (Kickingreder et al., 2016; Cui et al., 2015), and assessing response (Chow et al., 2014; Clarke et al., 1998). Related quantitative spatial analyses have demonstrated utility in predicting molecular subtypes (Yang et al., 2016) and survival (Czarnek et al., 2017; Mazurowski et al., 2014; Zhang et al., 2014) of glioblastoma patients. Given the availability of public imaging datasets such as The Cancer Imaging Archive (Clark et al., 2013), there is a clear need for the development of efficient and accurate segmentation utilities, which will allow for the systematic quantification of images in association with clinical and molecular characteristics.

1.1. Related Work

Manual segmentation is typically performed with 2D tools to delineate edges on each image slice. While manual segmentation is the gold standard (Porz et al., 2014), it is too time-consuming for large analyses, sometimes taking upwards of an hour per image series (Kaus et al., 2001). Because of this, many fully automatic and semi-automatic algorithms have been created to expedite the segmentation process. Reviews of these methods can be found in Bauer et al. (2013b) and Wang and Liu (2014). Benchmarks of fully automatic algorithms have demonstrated encouraging accuracies (Menze et al., 2015), but acceptance of these methods in the clinic is limited due to concerns about errors and transparency (Gordillo et al., 2013). Semi-automatic algorithms draw a balance by unifying the power of computer processing with the intuition of the human operator. However, existing semi-automatic programs still need improvement with regards to operator time (Fyllingen et al., 2016) and user-friendliness (Ramkumar et al., 2016).

1.2. Contribution

To address these drawbacks, this work provides and validates an accessible semi-automatic protocol for the fast segmentation of glioblastomas. Specific goals included the creation of an intuitive computer-assisted segmentation utility, addition of 3D editing tools for manual correction, and integration within a user-friendly environment. These aims were implemented in the Medical Imaging Interaction Toolkit (MITK) as an extension of its existing Segmentation plugin (Wolf et al., 2005; Maleike et al., 2009). This modified software, MITK with augmented tools for segmentation (MITKats), is also a free and open-source program. By addressing the aforementioned goals with MITKats, we expedite semi-automatic segmentation by introducing validated, easy-to-use 3D tools.

2. Methods

2.1. Data sources

A total of 38 3D MRIs of brain tumors were obtained from two publicly available datasets. 20 cases of high-grade gliomas (including glioblastomas and anaplastic astrocytomas) were obtained from the Multimodal Brain Tumor Segmentation Challenge (BRATS) 2012 (Menze et al., 2015), a notable accuracy benchmark. Four modalities were available for the BRATS dataset: T1, T1 with contrast (T1c), T2, and T2 FLAIR, though MITKats only used T1c and FLAIR images. The ground truths were derived from all four modalities and designated into 3 regions:

- Active: The contrast-enhancing parts of the tumor, seen on T1c
- Core: The Active component plus non-enhancing features seen on T1, including necrosis
- Whole: The hyper-intense region on T2 and FLAIR, corresponding to edema

18 cases of glioblastoma were obtained from a previously published study performed at St. Olav’s University Hospital (Fyllingen et al., 2016). Only T1c MRIs were used to create segmentations, which were generated in BrainVoyager (Goebel et al., 2006), 3D Slicer (Egger et al., 2013), and ITK-SNAP (Yushkevich et al., 2006). A single tumor region was labeled, comprising enhancing and necrotic regions. Given that the authors did not observe non-enhancing tumor regions, their definition of tumor was closest to that of the Core component from BRATS. While no ground truths were designated in this dataset, each segmentation was timed, serving as a speed benchmark.

Both datasets had originally been pre-processed, resulting in interpolation of image resolutions to a 1mm isotropic voxel size. Images from BRATS had been skull-stripped, while those from St. Olav’s had not.

2.2. Algorithmic Development

Two modifications were made to the MITK framework in order to expedite the segmentation process in MITKats. First, the Threshold Components tool was added, which expanded connected threshold segmentation to accept multiple seed points (and thus separated regions). It also allowed for the manipulation of seed points independently of the thresholds, as well as streamlining out unnecessary user input. The second modification was adding in segmentation capability to the Clipping Plane View, which was originally intended for volume measurements only. Therefore, a segmentation could be graphically adjusted in three dimensions through extraction of a clipped piece.

MITKats can be found here: <https://github.com/RabadanLab/MITKats>, and is in the process of being merged onto the main branch of MITK.

2.3. Segmentation Protocol

Segmentations were performed in MITKats by A.X.C., a medical student who had used similar software to segment 93 glioblastoma cases as part of a previous project (Crawford et al.). Segmentation time, as measured by stopwatch, was started after loading the original image(s) and stopped after opening the save segmentation dialog, thus ignoring the time for file operations.

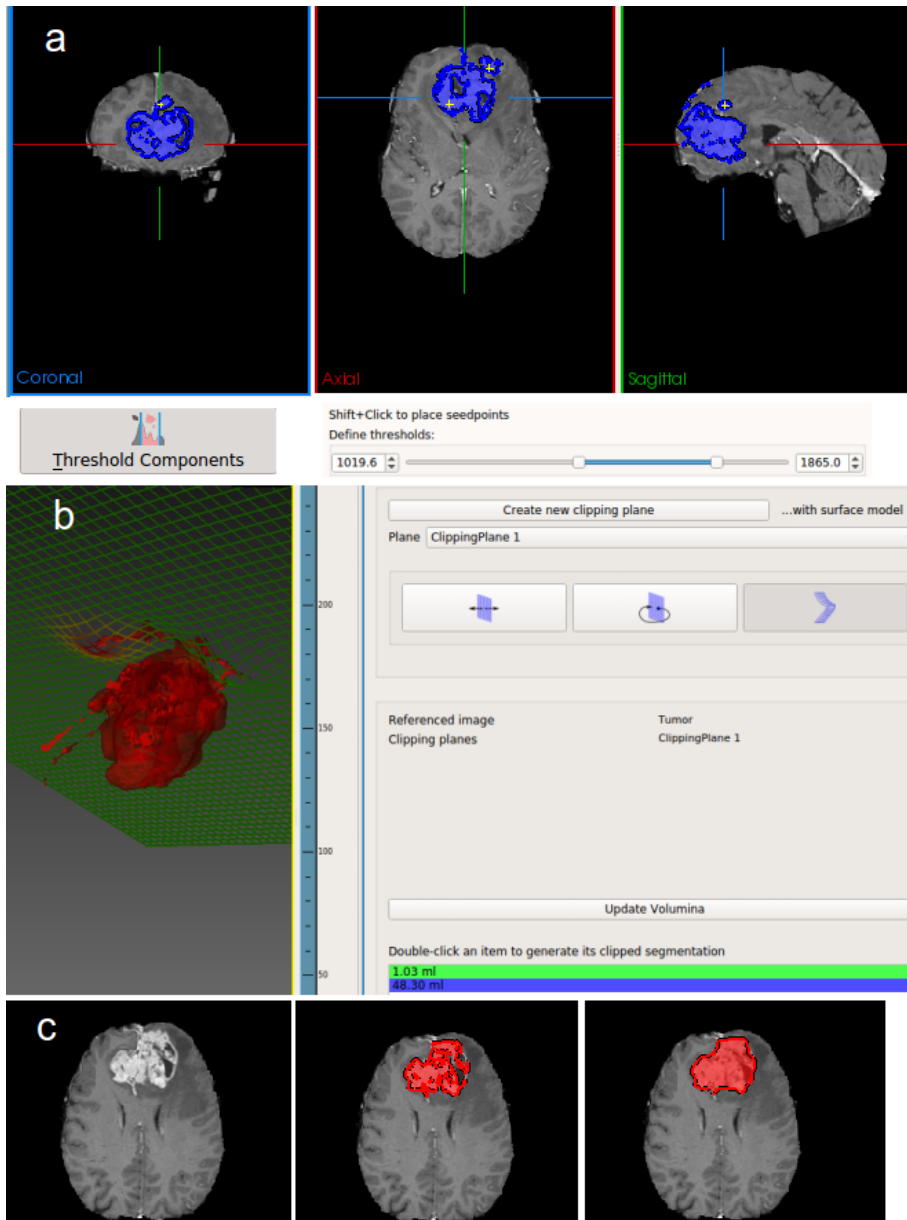


Figure 1: Demonstration of a user-friendly semiautomatic segmentation protocol.

a) The Threshold Components tool allows the user to set an intensity threshold and multiple seedpoints (yellow crosses). Regions within the threshold and connected to the seedpoints are selected. b) The deformable clipping plane allows 3D correction of the segmentation, typically useful for removing leaked regions. c) Original image, clipped image, and final morphological operations such as Closing and Fill Holes smooth the enhancing segmentation into a Core segmentation.

2.3.1. Thresholding

A new segmentation label was created for the T1c image, and the Segmentation plugin view is opened. Selecting the newly implemented Threshold Components tool, seed point(s) were placed in enhancing region(s), and the lower threshold adjusted until the apparent hyper-intensities were all included (Fig. 1a). If the tumor was grossly non-enhancing, another label was created where seed point(s) were placed in hypo-intense regions, and the upper threshold adjusted.

2.3.2. Cropping

Regions of normal brain tissue that were erroneously included as part of the Thresholding process were removed in two ways. Precise exclusion of regions was done via the Clipping Plane tool, where up to 6 deformable 3D surfaces were superimposed on the segmentation. This allowed the generalized separation of erroneous regions from the tumor body (Fig. 1b), a new feature added in MITKats. For gross corrections, the existing Image Cropping tool could be used instead. A 3D rectangular bounding box was graphically defined and used to mask and overwrite the original segmentation. Finally, if the true tumor contained only one connected component, either of these methods could be followed up with the Picking tool to exclude erroneous regions that were severed from the tumor.

2.3.3. Smoothing and Filling

The segmentation was smoothed via the Closing tool, a part of the existing set of Morphological Operations, typically with a radius of 2. This label was saved as the Active component. For the Core volume, the non-enhancing label could be joined to this component via the Union tool, if applicable. To include areas of necrosis, the Closing and Fill Holes tools were used (both typically with radius of 10), and this new label was saved as the Core component (Fig. 1c).

2.3.4. Whole Tumor

For segmenting the Whole tumor component of the BRATS dataset, the above protocol for obtaining the Core region was repeated for the FLAIR image.

2.4. Accuracy and Speed Analysis

The accuracy of MITKats segmentations was assessed by comparison to the reference segmentations provided by BRATS and St. Olav’s datasets. In BRATS, the references were ground truths fused from 4 expert manual annotations. Each of the Whole, Core, and Active components were compared to their reference counterparts via Dice score (Dice, 1945) as well as calculated tumor volume. The mean inter-rater Dice scores from BRATS were used as controls. This was because the fused ground truths were derived from the individual expert annotations, artificially bolstering the Dice score between any given expert and the fused standard.

For comparing data in the St. Olav’s cohort, the MITKats segmentations were assessed via Dice score and volume to all 12 reference segmentations (3 softwares \times 2 raters \times 2 repetitions). As a control, Dice scores were calculated only for pairs of reference segmentations created by different raters. The time to create the Core component of the MITKats segmentation was compared against the times reported in the dataset.

3. Results

Aggregate Dice scores and volume estimates of MITKats segmentations with respect to BRATS ground truths for each tumor region are shown in Table 1. The Dice similarity of MITKats segmentations compared to the ground truth was equivalent to inter-rater variability for the Whole and Active tumor regions, but was worse for the Core region. Volume measurements averaged over all regions were 94% of those estimated by the ground truth, with a mean fractional error of 18%.

A comparison of estimated volumes for each case across both datasets is shown in Figure 2, including a logarithmic Bland-Altman analysis. While the

Tumor Compartment		Whole	Core	Active
Dice Score (%)	MITKats v. BRATS	88±5	84±10	77±14
	BRATS Inter-rater	88±2	93±3	74±13
Volume Ratio		0.96	1.06	0.81
Volume Relative Error		10%	25%	20%

Table 1: Segmentation accuracy approaches inter-rater agreement in the Brain Tumor Segmentation Challenge. Twenty high-grade glioma cases were segmented using MITKats and compared against ground truths from BRATS. Three regions (Whole, Core, and Active) were segmented for each patient, and the mean Dice scores (\pm standard deviation) are shown. The volumes of each region were also compared to the ground truth.

volumes segmented by MITKats were similar to reference segmentations, they tended to be underestimated, particularly for the Active tumor region of the BRATS dataset.

The Core component of the MITKats segmentation was pairwise compared to segmentations performed by other softwares in the St. Olav dataset. The average Dice scores of MITKats segmentations compared to each of the reference segmentations was 0.88, compared against their inter-rater agreement of 0.94 (Figure 3a).

The time for segmentation is also compared to the St. Olav’s dataset in Figure 3b. The speed of MITKats as compared to those reported was an average of 4, 5, and 11 times faster than ITK-SNAP, 3D Slicer, and BrainVoyager, respectively. The typical Core segmentation using MITKats was 4.2 ± 2.0 minutes on the St. Olav’s dataset and 4.0 ± 3.1 minutes on the BRATS dataset, where uncertainties represent standard deviation.

4. Discussion and Conclusion

To our knowledge, this work is the first to validate the use of the MITK environment for the segmentation of brain tumors. Our modification MITKats provides fast and accurate segmentation, combining a semiautomatic tool with

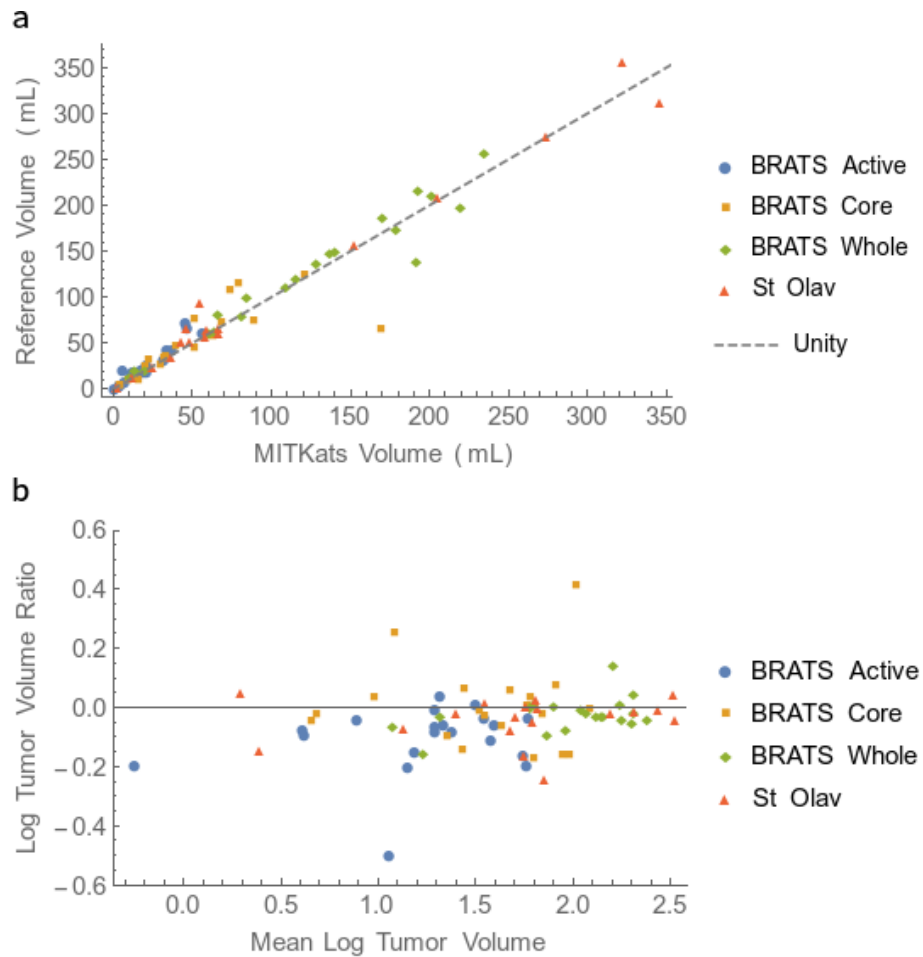


Figure 2: Comparison of segmented volumes by tumor region. a) Volumes calculated using MITKats are compared against their reference standards for each tumor component. (St. Olav segmentations designated only a single Core-like component.) b) A logarithmic Bland-Altman plot is shown for different regions of segmentations, comparing the ratio of segmented volumes to the averages of the base 10 logarithms of tumor volume (in mL). There is a tendency for MITKats to underestimate tumor volume at low sizes, particularly in the Active tumor component.

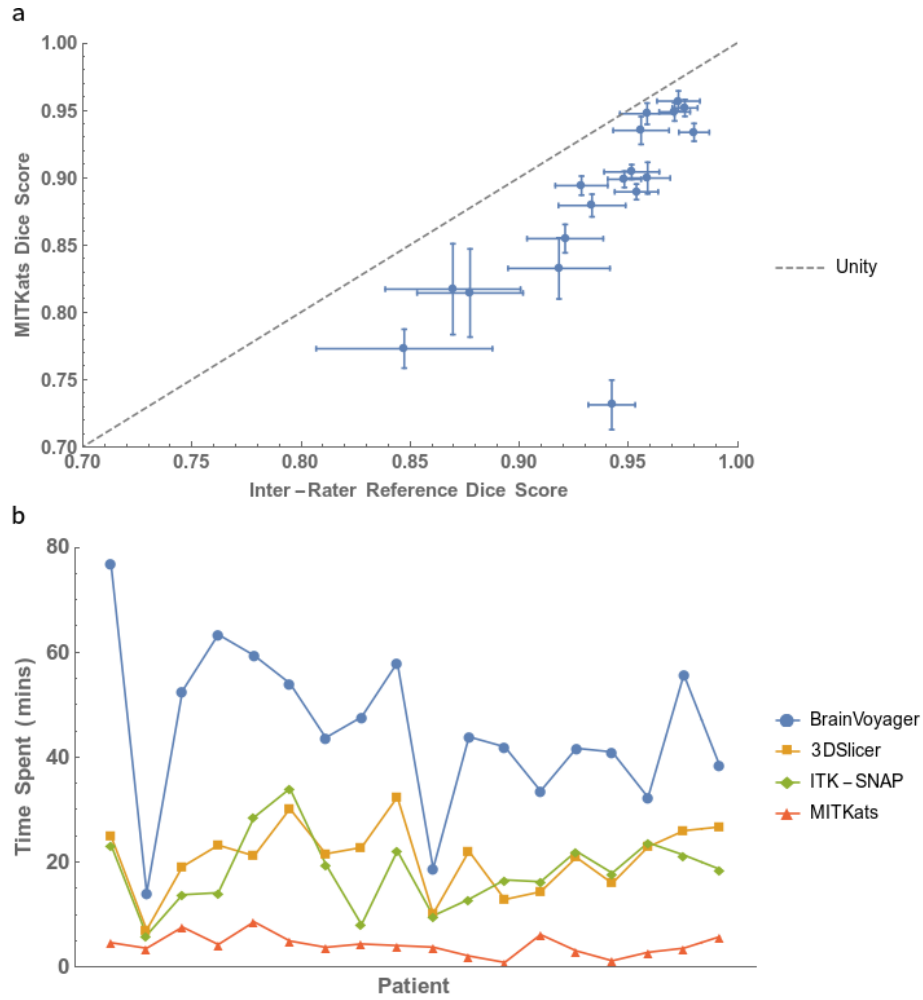


Figure 3: MITKats is faster than other segmentation softwares, while approaching optimal accuracy. a) Eighteen glioblastoma cases were segmented using MITKats and compared against the segmentations performed in Fyllingen et al. (2016). Points represent the average Dice score when compared to all other segmentations performed by different raters. Error bars represent standard deviation. b) The time required for segmenting via MITKats is compared to those using BrainVoyager, 3DSlicer, and ITK-SNAP (mean of 2 trials each).

flexible 3D editing, all wrapped in a user-friendly GUI. Benchmarking its accuracy against BRATS, it achieved a performance equal to inter-rater variability across Whole and Active tumor regions. The Core tumor region was somewhat lacking, perhaps due to our protocol not using T1 images, thus having different definitions for the component. Benchmarking its speed against the St. Olav’s dataset, MITKats was over 4 times faster than its quickest competitor. While its accuracy was somewhat lower than inter-rater variability, the reference segmentations were also semi-automatically derived, and therefore not necessarily the ground truth. Finally, MITK is an open source toolkit which encourages the free use and continued development of this software.

The scope of this work has some limitations with the protocol and datasets used. This pipeline works best for T1c and FLAIR imagery, because T1 without contrast has limited enhancement, and T2 enhancements are often the same intensity as cerebrospinal fluid. We hope to provide implementation for other modalities in the future as well as simultaneous multimodal analysis, which may benefit the accuracy of segmentations (Dupont et al., 2016). Providing support for perfusion and diffusion weighted images may also be particularly important for response assessment (Huang et al., 2015).

One note is that the BRATS dataset contained not just glioblastomas but also anaplastic astrocytomas, which are intermediates between GBMs and lower grade gliomas (LGGs). Given the satisfactory accuracy of segmenting this mixed dataset, this provides encouragement that MITKats could be extended to LGGs, which are typically harder to segment (Akkus et al., 2015). Eventual implementation and validation for LGGs and tumors outside the brain would be useful. Another point about the BRATS dataset is that the images were already skull-stripped, making the segmentation process somewhat easier. Integrating skull-stripping into our pipeline would be helpful for the user.

It is our belief that speed is not sufficiently emphasized in the current benchmarking of segmentation algorithms. While many studies report average segmentation times, the variability among different cases can be large. Within the datasets examined in this work, the fastest segmentation took less than a

minute, while the slowest took almost 11 minutes. Therefore, the individual listing of segmentation times is helpful for the direct comparison of algorithm speeds. We encourage future investigators to record both raw segmentations and operator time for each case to further advance this field.

References

- Akkus, Z., Sedlar, J., Coufalova, L., Korfiatis, P., Kline, T.L., Warner, J.D., Agrawal, J., Erickson, B.J., 2015. Semi-automated segmentation of pre-operative low grade gliomas in magnetic resonance imaging. *Cancer Imaging* 15, 1–10. doi:10.1186/s40644-015-0047-z.
- Bauer, S., Lu, H., May, C.P., Nolte, L.P., Büchler, P., Reyes, M., 2013a. Integrated segmentation of brain tumor images for radiotherapy and neurosurgery. *International Journal of Imaging Systems and Technology* 23, 59–63. doi:10.1002/ima.22037.
- Bauer, S., Wiest, R., Nolte, L.P., Reyes, M., 2013b. A survey of MRI-based medical image analysis for brain tumor studies. *Physics in Medicine and Biology* 58, R97–R129. doi:10.1088/0031-9155/58/13/R97.
- Chow, D.S., Qi, J., Guo, X., Miloushev, V.Z., Iwamoto, F.M., Bruce, J.N., Lassman, A.B., Schwartz, L.H., Lignelli, A., Zhao, B., Filippi, C.G., 2014. Semiautomated volumetric measurement on postcontrast MR imaging for analysis of recurrent and residual disease in glioblastoma multiforme. *American Journal of Neuroradiology* 35, 498–503. doi:10.3174/ajnr.A3724.
- Clark, K., Vendt, B., Smith, K., Freymann, J., Kirby, J., Koppel, P., Moore, S., Phillips, S., Maffitt, D., Pringle, M., Tarbox, L., Prior, F., 2013. The Cancer Imaging Archive (TCIA): Maintaining and Operating a Public Information Repository. *Journal of Digital Imaging* 26, 1045–1057. doi:10.1007/s10278-013-9622-7.

- Clarke, L.P., Velthuizen, R.P., Clark, M., Gaviria, J., Hall, L., Goldgof, D., Murtagh, R., Phuphanich, S., Brem, S., 1998. MRI measurement of brain tumor response: comparison of visual metric and automatic segmentation. *Magnetic resonance imaging* 16, 271–279. doi:10.1016/S0730-725X(97)00302-0.
- Crawford, L., Monod, A., Chen, A.X., Mukherjee, S., Rabadán, R., . Topological Summaries of Tumor Images Improve Prediction of Disease Free Survival in Glioblastoma Multiforme. Arxiv pre-print URL: <http://arxiv.org/abs/1611.06818>, arXiv:1611.06818.
- Cui, Y., Tha, K.K., Terasaka, S., Yamaguchi, S., Wang, J., Kudo, K., Xing, L., Shirato, H., Li, R., 2015. Prognostic Imaging Biomarkers in Glioblastoma: Development and Independent Validation on the Basis of Multiregion and Quantitative Analysis of MR Images. *Radiology* 000, 150358. doi:10.1148/radiol.2015150358.
- Czarnek, N., Clark, K., Peters, K.B., Mazurowski, M.A., 2017. Algorithmic three-dimensional analysis of tumor shape in MRI improves prognosis of survival in glioblastoma: a multi-institutional study. *Journal of Neuro-Oncology* 132, 55–62. doi:10.1007/s11060-016-2359-7.
- DeAngelis, L.M., 2001. Brain Tumors. *New England Journal of Medicine* 344, 114–123. doi:10.1056/NEJM200101113440207.
- Dice, L.R., 1945. Measures of the Amount of Ecologic Association Between Species. *Ecology* 26, 297–302. doi:10.2307/1932409.
- Dupont, C., Betrouni, N., Reyns, N., Vermandel, M., 2016. On image segmentation methods applied to glioblastoma : State of art and new trends. *IRBM* 1, 1–13. doi:10.1016/j.irbm.2015.12.004.
- Egger, J., Kapur, T., Fedorov, A., Pieper, S., Miller, J.V., Veeraraghavan, H., Freisleben, B., Golby, A.J., Nimsy, C., Kikinis, R., 2013. GBM volumetry using the 3D Slicer medical image computing platform. *Sci Rep* 3, 1364. doi:10.1038/srep01364.

- Fyllingen, E.H., Stensjoen, A.L., Berntsen, E.M., Solheim, O., Reinertsen, I., 2016. Glioblastoma segmentation: Comparison of three different software packages. *PLoS ONE* 11. doi:10.1371/journal.pone.0164891.
- Goebel, R., Esposito, F., Formisano, E., 2006. Analysis of Functional Image Analysis Contest (FIAC) data with BrainVoyager QX: From single-subject to cortically aligned group General Linear Model analysis and self-organizing group Independent Component Analysis. *Human Brain Mapping* 27, 392–401. doi:10.1002/hbm.20249.
- Gordillo, N., Montseny, E., Sobrevilla, P., 2013. State of the art survey on MRI brain tumor segmentation. *Magnetic Resonance Imaging* 31, 1426–1438. doi:10.1016/j.mri.2013.05.002.
- Huang, R.Y., Neagu, M.R., Reardon, D.A., Wen, P.Y., 2015. Pitfalls in the neuroimaging of glioblastoma in the era of antiangiogenic and immuno/targeted therapy - detecting illusive disease, defining response. *Frontiers in Neurology* 6, 1–16. doi:10.3389/fneur.2015.00033.
- Kaus, M.R., Warfield, S.K., Nabavi, A., Black, P.M., Jolesz, F.A., Kikinis, R., 2001. Automated segmentation of MR images of brain tumors. *Radiology* 218, 586–591. doi:10.1148/radiology.218.2.r01fe44586.
- Kickingreder, P., Burth, S., Wick, A., Götz, M., Eidel, O., Schlemmer, H.P., Maier-Hein, K.H., Wick, W., Bendszus, M., Radbruch, A., Bonekamp, D., 2016. Radiomic Profiling of Glioblastoma: Identifying an Imaging Predictor of Patient Survival with Improved Performance over Established Clinical and Radiologic Risk Models. *Radiology* 280, 880–889. doi:10.1148/radiol.2016160845.
- Mabray, M.C., Barajas, R.F., Cha, S., 2015. Modern brain tumor imaging. *Brain tumor research and treatment* 3, 8–23. doi:10.14791/btrt.2015.3.1.8.
- Maleike, D., Nolden, M., Meinzer, H.P., Wolf, I., 2009. Interactive segmentation

- framework of the Medical Imaging Interaction Toolkit. *Computer Methods and Programs in Biomedicine* 96, 72–83. doi:10.1016/j.cmpb.2009.04.004.
- Mazurowski, M.A., Zhang, J., Peters, K.B., Hobbs, H., 2014. Computer-extracted MR imaging features are associated with survival in glioblastoma patients. *Journal of Neuro-Oncology* 120, 483–488. doi:10.1007/s11060-014-1580-5.
- Menze, B.H., Jakab, A., Bauer, S., Kalpathy-Cramer, J., Farahani, K., Kirby, J., Burren, Y., Porz, N., Slotboom, J., Wiest, R., Lanczi, L., Gerstner, E., Weber, M.A., Arbel, T., Avants, B.B., Ayache, N., Buendia, P., Collins, D.L., Cordier, N., Corso, J.J., Criminisi, A., Das, T., Delingette, H., Demiralp, a., Durst, C.R., Dojat, M., Doyle, S., Festa, J., Forbes, F., Geremia, E., Glocker, B., Golland, P., Guo, X., Hamamci, A., Iftekharuddin, K.M., Jena, R., John, N.M., Konukoglu, E., Lashkari, D., Mariz, J.A., Meier, R., Pereira, S., Precup, D., Price, S.J., Raviv, T.R., Reza, S.M.S., Ryan, M., Sarikaya, D., Schwartz, L., Shin, H.C., Shotton, J., Silva, C.A., Sousa, N., Subbanna, N.K., Szekely, G., Taylor, T.J., Thomas, O.M., Tustison, N.J., Unal, G., Vasseur, F., Wintermark, M., Ye, D.H., Zhao, L., Zhao, B., Zikic, D., Prastawa, M., Reyes, M., Van Leemput, K., 2015. The Multimodal Brain Tumor Image Segmentation Benchmark (BRATS). *IEEE Transactions on Medical Imaging* 34, 1993–2024. doi:10.1109/TMI.2014.2377694.
- Porz, N., Bauer, S., Pica, A., Schucht, P., Beck, J., Verma, R.K., Slotboom, J., Reyes, M., Wiest, R., 2014. Multi-modal glioblastoma segmentation: Man versus machine. *PLoS ONE* 9, 1–9. doi:10.1371/journal.pone.0096873.
- Ramkumar, A., Dolz, J., Kirisli, H.A., Adebahr, S., Schimek-Jasch, T., Nestle, U., Massoptier, L., Varga, E., Stappers, P.J., Niessen, W.J., Song, Y., 2016. User Interaction in Semi-Automatic Segmentation of Organs at Risk: a Case Study in Radiotherapy. *Journal of Digital Imaging* 29, 264–277. doi:10.1007/s10278-015-9839-8.
- Wang, J., Liu, T., 2014. A survey of MRI-based brain tumor segmentation

- methods. *Tsinghua Science and Technology* 19, 578–595. doi:10.1109/TST.2014.6961028.
- Wolf, I., Vetter, M., Wegner, I., Bottger, T., Nolden, M., Schobinger, M., Hastenteufel, M., Kunert, T., Meinzer, H.P., 2005. The medical imaging interaction toolkit. *Medical Image Analysis* 9, 594–604. doi:10.1016/j.media.2005.04.005.
- Yang, D., Rao, G., Martinez, J., Veeraraghavan, A., Rao, A., Yang, D., 2016. Evaluation of tumor-derived MRI-texture features for discrimination of molecular subtypes and prediction of 12-month survival status in glioblastoma Evaluation of tumor-derived MRI-texture features for discrimination of molecular subtypes and prediction o 6725. doi:10.1118/1.4934373.
- Yushkevich, P.A., Piven, J., Hazlett, H.C., Smith, R.G., Ho, S., Gee, J.C., Gerig, G., 2006. User-guided 3D active contour segmentation of anatomical structures: Significantly improved efficiency and reliability. *NeuroImage* 31, 1116–1128. doi:10.1016/j.neuroimage.2006.01.015.
- Zhang, Z., Jiang, H., Chen, X., Bai, J., Cui, Y., Ren, X., Chen, X., Wang, J., Zeng, W., Lin, S., 2014. Identifying the survival subtypes of glioblastoma by quantitative volumetric analysis of MRI. *Journal of Neuro-Oncology* 119, 207–214. doi:10.1007/s11060-014-1478-2.

Acknowledgments

We would like to thank Anthea Monod and the rest of the Rabadan lab for their helpful comments and feedback. A.X.C. is funded by NIH grant T32GM007367 as part of the Medical Scientist Training Program (MSTP). R.R. acknowledges funding from the NIH (U54 CA193313, R01 CA185486, R01 CA179044).